Hindawi Publishing Corporation
Journal of Nanomaterials
Volume 2015, Article ID 389594, 7 pages
http://dx.doi.org/10.1155/2015/389594

Research Article

Formation of Ultrafine-Grained Ti_3Al on a Ti48Al2Cr2Nb Intermetallic Alloy Induced by Pulsed Electron Beam Treatment

Jiawei Dong, Kemin Zhang, Yang Cai, Zhimin Zhang, Yuan Lei, and Tao Zhang

School of Materials Engineering, Shanghai University of Engineering Science, Shanghai 201620, China

Correspondence should be addressed to Kemin Zhang; zhangkm@sues.edu.cn

Received 2 September 2014; Revised 4 March 2015; Accepted 5 March 2015

Academic Editor: Thierry Grosdidier

The microstructure modifications, phase, and texture formations encountered in a TiAl based Ti48Al2Cr2Nb intermetallic alloy induced by the high current pulsed electron beam (HCPEB) treatment were carefully investigated using scanning electron microscope (SEM), X-ray diffraction (XRD), and electron backscattered diffraction (EBSD) techniques. The initial material contains the majority γ-TiAl phase and the minority α-Ti_3Al phase. After the HCPEB treatment, the initial α-Ti_3Al was dissolved into the melted layer and the very top surface is covered by ultrafine-grained α-Ti_3Al phase having thermal stress induced cracks. EBSD analyses showed that α-Ti_3Al phase on the very top surface has a $\langle 001 \rangle$//ND fiber texture and its texture intensity increases with the number of pulses. The superfast thermal stress cycles and the selective evaporation induced by the HCPEB treatment account for the microstructure modifications and formations of ultrafine α-Ti_3Al in the TiAl based intermetallic alloy.

1. Introduction

Surface treatment techniques are widely used in different industries for improving the performances and prolonging service time of materials. In the past decades, pulsed energetic beams, such as laser, ion, and electron beams, have attracted much attention in the field of materials surface modifications due to their advantages, including the high efficiency, less energy consumption, and environmentally friendly nature [1–4]. Among these pulsed beam surface modification techniques, the high current pulsed electron beam (HCPEB) [2, 5–8] is considered as a promising technique for surface modifications of metallic materials with high potential for industrial applications. Its main feature is the generation of an electron beam with low energy (10~35 keV), short pulse (~1 μs), and high peak current density (~10^4 A/cm^2). The interaction of the pulsed electron beam with the material introduces very fast heating and melting in the surface layer of the material that is followed by a rapid cooling process due to the heat conduction towards the cold substrate [8–10]. These nonequilibrium processes can easily change the microstructures, chemical compositions, phase components, and stress states at the surface. It has been established in many previous works that the hardness, corrosion, and wear resistances of the material surfaces can be significantly improved by this treatment when proper treatment modes and parameters are applied on the materials [5–10]. The improved surface properties can be mainly attributed to the formation of ultrafine grains/precipitates formed from the highly undercooled melt [9, 10], metastable phase transformations [11–13], selective surface purification [14], and strain hardening induced by the thermal stress waves [15, 16]. It is also established that partial evaporation may occur at the top surface layer and can be intensive when the energy density of the electron beam is sufficiently high [17–19]. This phenomenon can modify significantly the melt chemistry [11, 19] and was also suggested to lead to the development of specific solidification texture in the rapidly solidified layer [11].

Recently, the HCPEB treatment was applied to intermetallic compounds [13, 20–22]. Under the so-called heating mode (no surface melting), the surface hardness of a FeAl alloy increased due to the formation of defects and the grain refinement while good corrosion properties were kept [20]. Also, the texture in the surface layer of the FeAl alloy

was modified by the HCPEB treatment under the heating mode, which was attributed to the repeated deformation and recrystallization/recovery induced by thermal cycles in the treated surface layer. TiAl based alloys are also important intermetallics used in aeronautic industry. Their surface properties are very important in determining their lifetime. In recent studies, TiAl surfaces were synthesized by cyclic pulsed melting/mixing of predeposited Al film (100 nm) on a Ti substrate using HCPEB [13, 21, 22]. The amount of Al introduced into Ti was sufficiently limited to remain on the Ti/Ti_3Al side of the phase diagram and led to a crack-free surface [13, 21]. The surface analysis has revealed the complexity of the local transformation paths associated with this synthesis mode [22]. A fairly good surface chemical homogeneity was obtained but duplex microstructures formed because of local changes in the primary phase under rapid solidification and the subsequent modifications of the solid state transformation paths [22]. While these TiAl based surfaces were prepared by complex mixing processes, the effects of the direct HCPEB treatment of a TiAl alloy on the phase transformations, microstructure, and texture modifications have not been well investigated yet.

2. Experimental

The TiAl based intermetallic alloy studied in the present work is the well known Ti48Al2Cr2Nb alloy. Specimens of the alloy were cut into 2 mm-thick discs and their surfaces were polished down to diamond paste of 1 μm prior to the HCPEB treatment. Figure 1 shows a typical scanning electron microscope (SEM) image taken on the untreated TiAl alloy sample under backscattered electron (BSE) condition. The initial material contains two phases, namely, γ-TiAl phase having large grains in dark contrast and α-Ti_3Al grains in bright contrast located at the grain boundaries, as arrowed in Figure 1. Details about the microstructure and processing of this alloy can be obtained in [23]. The HCPEB parameters used in the present work were as follows: the accelerating voltage 27 kV, the energy density ~2.5 J/cm^2. The TiAl samples were treated for 5 and 20 pulses with pulse duration of 1.5 μs. The dwell time between each pulse was 10 s.

A JEOL 6500F type field emission gun scanning electron microscope (FEG-SEM) equipped with an electron backscattered diffraction (EBSD) attachment was used to gain information about the microstructure, phase, and texture states of the investigated materials. For EBSD analyses, the SEM was operated at 15 kV with the sample tilted by 70°. Under this condition, the EBSD results give the texture information only in the very top surface layer of about several nms. The step size used for measurements is 50 nm. Conventional X-ray diffraction (θ-2θ mode) was carried out using a SHIMADZU XRD-6000 apparatus equipped with a Cu-K_α radiation source to analyze the phase state at the sample surface.

3. Results

Figure 2 shows the XRD patterns of the untreated and HCPEB treated TiAl alloy samples. The XRD pattern of the untreated material (Figure 2(a)) confirmed the presence of the majority γ-TiAl phase and the minority α-Ti_3Al phase. After the HCPEB treatments (both 5 and 20 pulses), the XRD patterns shown in Figures 2(b) and 2(c) can be also indexed using γ-TiAl and α-Ti_3Al phases. However, the intensity of those diffraction peaks corresponding to the γ-TiAl phase has been reduced sharply compared to those from the α-Ti_3Al phase, indicating that the volume fraction of α-Ti_3Al phase in the surface layer has increased over the γ-TiAl one after the HCPEB treatments.

Figure 3 shows some SEM images taken from the surface of the HCPEB treated samples. Figure 3(a) is a low magnification SEM image of the 5-pulsed sample obtained under BSE condition. It reveals two distinct features after the HCPEB treatment. One is the presence of cracks. These cracks, which witness the intrinsic brittleness of the intermetallic phases, are generated by the tensile stress during cooling [24]. The other is the wavy morphology of the surface, which is a typical feature of the materials treated by HCPEB under

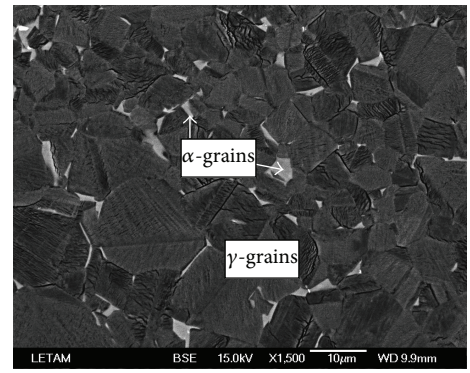

Figure 1: SEM image of the untreated TiAl alloy sample under backscattered electron condition.

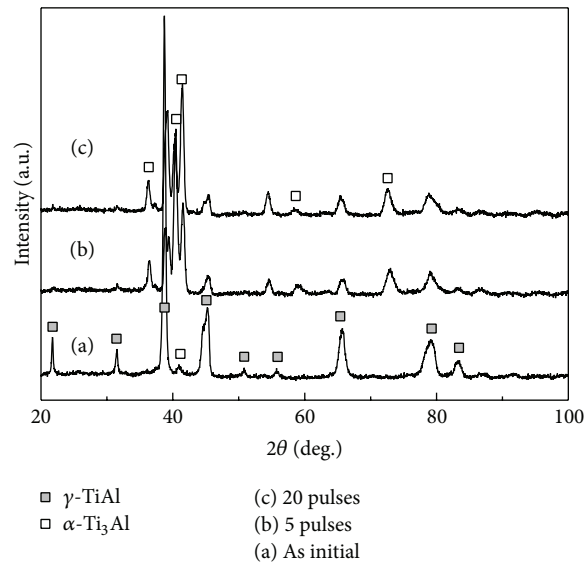

Figure 2: XRD patterns of untreated (a) and the HCPEB treated Ti48Al2Cr2Nb alloy samples with 5 pulses (b) and 10 pulses (c).

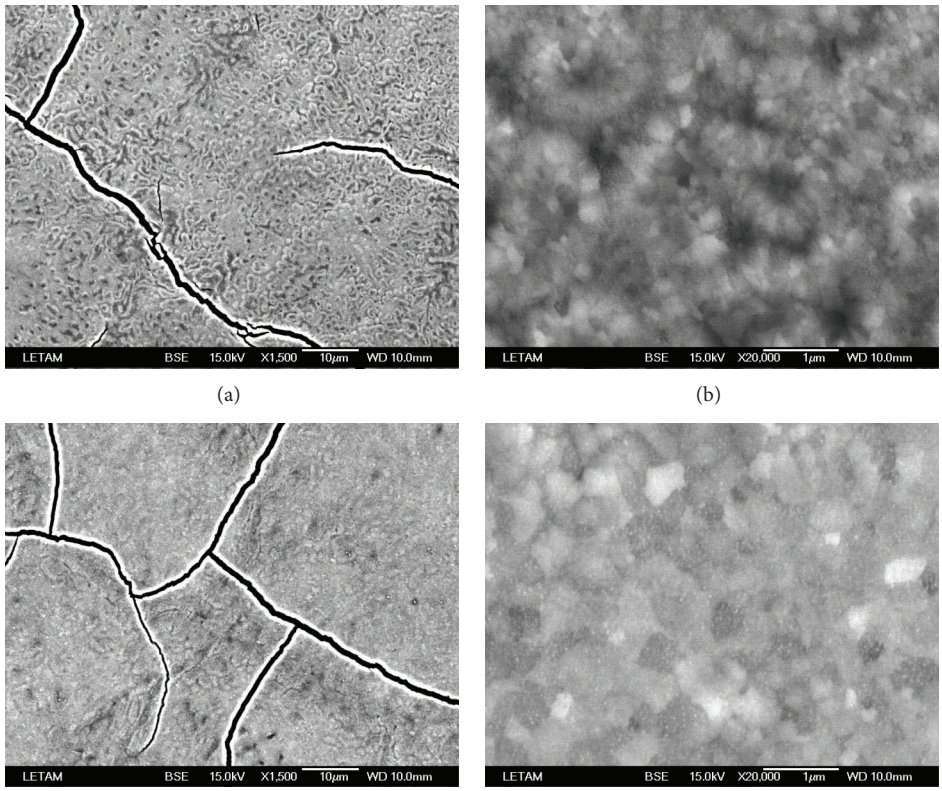

Figure 3: Typical SEM images taken on the surface of the HCPEB treated samples under backscattered condition. (a) 5 pulses, low magnification; (b) 5 pulses, high magnification; (c) 20 pulses, low magnification; (d) 20 pulses, high magnification.

the evaporating mode [11, 17, 19]. Figure 3(b) gives a high magnification BSE image of the 5-pulsed sample. It shows that very fine grains, having size in the range from 100 nm to 200 nm, covered the whole surface. Figures 3(c) and 3(d) show another set of low and high magnification SEM images taken on the 20-pulsed sample. These images reveal quite similar features: the cracks, the wavy aspect of the surface, and the fine grain structure.

Figure 4 shows a BSE cross section micrograph of the 20-pulsed sample. Within the substrate, the γ-TiAl phase has a deep grey contrast while the small fraction of α-Ti_3Al appears with a brighter contrast. At the upper part of the material, the melted zone has also a bright contrast and its depth is about 4 to 5 μm. Two layers can actually be depicted within the melted zone. The very top surface of the melted layer, around 500 nm in depth, is characterized by very fine grains having size of about 100 nm. This observation is consistent with the results shown in Figure 3(d) that fine grains cover the HCPEB treated surface. Underneath is present a layer having subtle differences in the shade of gray but within which no specific contrast of fine grain structure can be distinguished. The differences in shade of grey, which are correlated to the local presence of the α-Ti_3Al within the subsurface, suggest differences in local chemistry which generally witness the dissolution process during melting under HCPEB [25–27]. The formation of such kind of brighter contrast is due to the diffusion of Ti from the α-Ti_3Al towards the surrounding areas, which also explains the brighter contrast of the top surface melted layer.

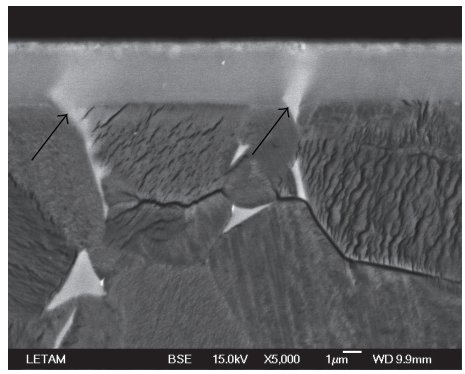

Figure 4: A typical cross section SEM image of the TiAl sample HCPEB treated with 20 pulses under backscattered condition.

To gain more information about the microstructure, phase component, and texture in the surface melted zone, EBSD analyses were carried out at the top surface of the treated samples and the results are given in Figure 5. The corresponding color triangle is shown inset. It can be observed from Figures 5(a) and 5(c) that the rapid solidification has led to a fine grain structure. The mean grain size was estimated to be around 190 nm and 430 nm after 5 and 20 pulses,

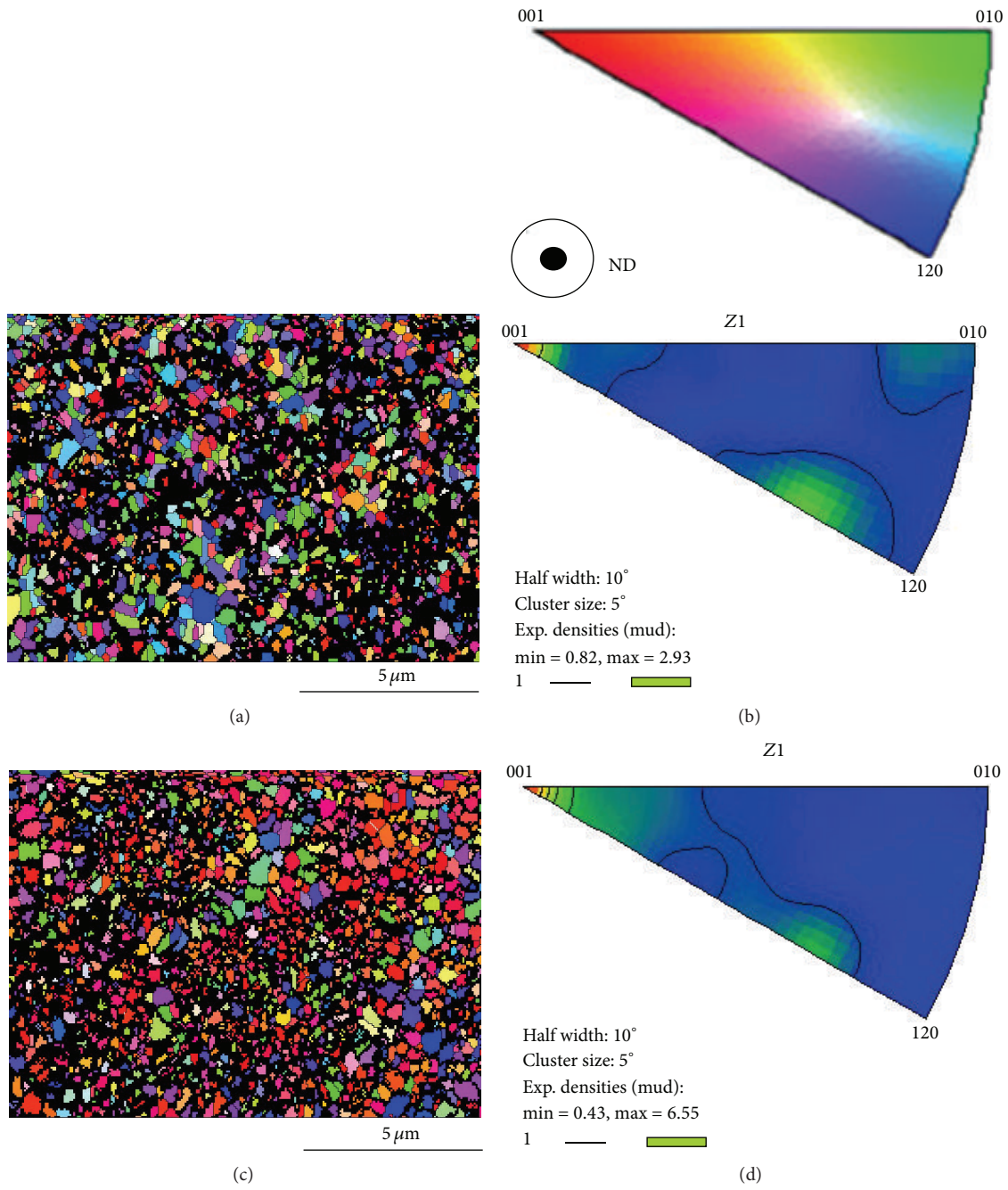

FIGURE 5: Typical EBSD orientation maps taken on the surface of the TiAl sample HCPEB treated with 5 (a) and 20 (c) pulses and the corresponding inverse pole figures for 5-pulsed (b) and 20-pulsed (d) samples. Standard color triangle is shown inset.

respectively. All the grains on the very top surface were indexed as corresponding to the α-Ti_3Al phase having the hexagon structure and no γ-TiAl phase could be indexed after 5 or 20 pulses. Therefore, the very top surfaces are essentially covered by the α-Ti_3Al fine grain layer after the HCPEB treatment. It should be noted here that the dark areas in the EBSD maps are areas having a low quality of Kikuchi patterns or no pattern at all. These areas of poor indexing may correspond to extremely fine grains, constrained areas present at the grain boundaries, or amorphous domains possibly due to some pollution of the rapidly solidified TiAl based melt [28]. The inverse pole figures in Figures 5(b) and 5(d) clearly show, for both treatments (5 and 20 pulses), a major ⟨001⟩ fiber of the α-Ti_3Al parallel to the sample normal direction (ND). After 5 pulses, the fiber has a maximum intensity of 2.9 times of random texture while its strength increases to 6.5 times of random texture after 20 pulses. Indeed, the orientation map in Figure 5(c) is strongly dominated by grains having a red color, which correspond to grains having their {001} planes perpendicular to ND.

4. Discussions

During the HCPEB treatment, the electron beam energy is mainly transferred into heat when electrons are acting with the treated materials, which induces dynamic temperature fields in the surface layers. By using computer simulation developed in previous works [15, 19], it is possible to estimate the temperature field within a pulse duration of the HCPEB treatment process. The application of this computing procedure to the present case of the Ti48Al2Cr2Nb alloy gave the maximum temperature reached at the top surface to be about 2800 K. This is far exceeding the melting point of this alloy (~1783 K) and in the range of its boiling point. As a consequence, the species (Ti, Al, Cr, and Nb) present on the top surface layer have the potential to evaporate into the vacuum chamber during the HCPEB treatment. Among these elements, Al has the lowest melting (933 K) and boiling (2793 K) points as well as the smallest heat of vaporization (293 kJ/mol). Therefore, a selective evaporation of Al over other elements occurs under the HCPEB treatment of the Ti48Al2Cr2Nb alloy, resulting in the depletion of Al in the top surface layer [19]. The composition analyses given in a previous work have shown that the Al concentration at the top surface reduces to 44 wt% after 5 pulses and further decreases to 42 wt% after 20 pulses [19]. Such kind of selective evaporation was also observed in Mg alloys [17], NiTi alloys [11, 29], and a near α-Ti alloy [18] treated by HCPEB under the "evaporating mode." The evaporation occurring at the top surface accounts for the presence of wavy morphology of the treated surface. Moreover, the reduced concentration of Al also favours the formation of the α-Ti_3Al phase at the top surface.

After melting and evaporation, rapid solidification occurs in the melted layer at rates as high as 10^7 K/s due to the heat conduction towards the substrate [18]. This, together with the selective evaporation of Al, leads to the formation of ultrafine α-Ti_3Al grains instead of γ-TiAl grains at the very top surface layer. The EBSD analyses revealed the presence of a ⟨001⟩//ND fiber texture for the rapidly solidified α-Ti_3Al layer at the very top surface that strengthens with the number of pulses. The presence of texture in the melted layer of HCPEB treated metals has been revealed by various authors. Contrary to what was observed in several treated metals such as NiTi [11], the 316L stainless steel [30–32], the AISI 310 precipitation hardening steel [33], and the FeAl alloys treated under the heating mode [20], the texture developed in the top surface of HCPEB treated TiAl alloy is the normal ⟨001⟩//ND fiber texture. The texture development during solidification is usually influenced by the initial nucleation process and the following grain growth. As the HCPEB process leads to a resolidification onto an unmelted substrate, the nucleation stage could be affected by the orientation of the substrate material from which the melted layer resolidifies. However, as can be seen from the cross section SEM image of the 20-pulsed sample (Figure 4), it appears that the small grains only exist in the top surface layer. Thus the texture of the fine-grained α-Ti_3Al layer at the very top surface cannot be affected by the unmelted substrate. Generally, a growth process is done along the thermal gradient direction following well defined crystallographic directions which, for hexagonal materials, are the ⟨001⟩ directions [34]. This can also be the case under rapid solidification conditions. Temperature simulations reveal that the solidification rate reduces from the bottom of the melted layer towards to the top. Therefore, at the top surface layer, grains have longer durations to grow larger when compared with the grains at the bottom of the melted layer. After higher number of pulses, the melted layer depth increases and heat conductivity in the surface layer decreases due to the defects generated by repeated energy input [9]. As a result, the solidification rate in the top surface also reduces with the increasing number of pulses, providing longer time for grain growth. This explains the fact that both the average grain size and the texture intensity of the α-Ti_3Al at the very top surface increase with the increasing the number of pulses.

5. Conclusions

The modifications in microstructure, phase components, and texture development have been investigated in a TiAl base alloy after the HCPEB treatment under evaporation mode. The evaporation occurring in the surface layer has created a wavy aspect on the surface and a selective evaporation of Al over other elements in the treated Ti48Al2Cr2Nb alloy. This has resulted in a decrease in the Al concentration at the surface and the formation of the α-Ti_3Al rich microstructure in the melted layer. The superfast solidification has led to the formation of ultrafine-grained α-Ti_3Al layer on the very top surface. This layer has a ⟨001⟩//ND fiber texture developed during solidification. Both the average grain size and the texture intensity of the α-Ti_3Al phase at the very top surface increased when the number of pulses was increased from 5 to 20.

Conflict of Interests

The authors declare that there is no conflict of interests regarding the publication of this paper.

Acknowledgments

Professor Kemin Zhang would like to acknowledge Shanghai University of Engineering Science Innovation Fund for Graduate Students (no. 13KY0501) and Shanghai Innovation Fund for Undergraduate Students (no. cs 1305005). This work is supported by the National Natural Science Foundation (nos. 51101096, 51271121). The authors would like to thank Dr. Nathalie Gey and Professor Thierry Grosdidier from Laboratoire d'Etude des Microstructures et de Mécanique des Matériaux (LEM3) for their help in EBSD measurements. This work is carried out in the framework of the French Laboratoire d'Excellence "Labex DAMAS."

References

[1] M. Sorescu, "The role of magnetostriction in pulsed laser irradiation of amorphous alloys," *Journal of Alloys and Compounds*, vol. 280, no. 1-2, pp. 251–254, 1998.

[2] D. I. Proskurovsky, V. P. Rotshtein, G. E. Ozur et al., "Pulsed electron-beam technology for surface modification of metallic materials," *Journal of Vacuum Science and Technology A: Vacuum, Surfaces and Films*, vol. 16, no. 4, pp. 2480–2488, 1998.

[3] X. Y. Le, S. Yan, W. J. Zhao, B. X. Han, Y. G. Wang, and J. M. Xue, "Computer simulation of thermal-mechanical effects of high intensity pulsed ion beams on a metal surface," *Surface and Coatings Technology*, vol. 128-129, no. 1, pp. 381–387, 2000.

[4] V. Engelko, G. Mueller, A. Rusanov et al., "Surface modification/alloying using intense pulsed electron beam as a tool for improving the corrosion resistance of steels exposed to heavy liquid metals," *Journal of Nuclear Materials*, vol. 415, no. 3, pp. 270–275, 2011.

[5] D. I. Proskurovsky, V. P. Rotshtein, G. E. Ozur, Y. F. Ivanov, and A. B. Markov, "Physical foundations for surface treatment of materials with low energy, high current electron beams," *Surface and Coatings Technology*, vol. 125, no. 1–3, pp. 49–56, 2000.

[6] C. Dong, A. Wu, S. Hao et al., "Surface treatment by high current pulsed electron beam," *Surface and Coatings Technology*, vol. 163-164, pp. 620–624, 2003.

[7] Y.-K. Gao, "Influence of pulsed electron beam treatment on microstructure and properties of TA15 titanium alloy," *Applied Surface Science*, vol. 264, pp. 633–635, 2013.

[8] X. D. Zhang, S. Z. Hao, X. N. Li, C. Dong, and T. Grosdidier, "Surface modification of pure titanium by pulsed electron beam," *Applied Surface Science*, vol. 257, no. 13, pp. 5899–5902, 2011.

[9] J. X. Zou, T. Grosdidier, K. M. Zhang, and C. Dong, "Mechanisms of nanostructure and metastable phase formations in the surface melted layers of a HCPEB-treated D2 steel," *Acta Materialia*, vol. 54, no. 20, pp. 5409–5419, 2006.

[10] J. X. Zou, T. Grosdidier, B. Bolle, K. M. Zhang, and C. Dong, "Texture and microstructure at the surface of an AISI D2 steel treated by high current pulsed electron beam," *Metallurgical and Materials Transactions A: Physical Metallurgy and Materials Science*, vol. 38, no. 9, pp. 2061–2071, 2007.

[11] K. M. Zhang, J. X. Zou, T. Grosdidier et al., "Mechanisms of structural evolutions associated with the high current pulsed electron beam treatment of a NiTi shape memory alloy," *Journal of Vacuum Science and Technology A: Vacuum, Surfaces and Films*, vol. 25, no. 1, pp. 28–36, 2007.

[12] S. Z. Hao, B. Gao, A. M. Wu et al., "Surface modification of steels and magnesium alloy by high current pulsed electron beam," *Nuclear Instruments and Methods in Physics Research Section B: Beam Interactions with Materials and Atoms*, vol. 240, no. 3, pp. 646–652, 2005.

[13] V. P. Rotshtein, Yu. F. Ivanov, Yu. A. Kolubaeva et al., "Synthesis of Ti3Al and TiAl based surface alloys by pulsed electron-beam melting of Al(film)/Ti(substrate) system," *Technical Physics Letters*, vol. 37, no. 3, pp. 226–229, 2011.

[14] J. X. Zou, K. M. Zhang, C. Dong, Y. Qin, S. Hao, and T. Grosdidier, "Selective surface purification via crater eruption under pulsed electron beam irradiation," *Applied Physics Letters*, vol. 89, no. 4, Article ID 041913, 2006.

[15] Y. Qin, C. Dong, Z. Song et al., "Deep Modification of materials by thermal stress wave generated by irradiation of high-current pulsed electron beams," *Journal of Vacuum Science & Technology A*, vol. 27, no. 3, pp. 430–435, 2009.

[16] J. X. Zou, K. M. Zhang, S. Z. Hao, C. Dong, and T. Grosdidier, "Mechanisms of hardening, wear and corrosion improvement of 316 L stainless steel by low energy high current pulsed electron beam surface treatment," *Thin Solid Films*, vol. 519, no. 4, pp. 1404–1415, 2010.

[17] J. Cai, S. Z. Yang, L. Ji, Q. F. Guan, Z. P. Wang, and Z. Y. Han, "Surface microstructure and high temperature oxidation resistance of thermal sprayed CoCrAlY coating irradiated by high current pulsed electron beam," *Surface and Coatings Technology*, vol. 251, pp. 217–225, 2014.

[18] X. D. Zhang, J. X. Zou, S. Weber, S. Z. Hao, C. Dong, and T. Grosdidier, "Microstructure and property modifications in a near alpha Ti alloy induced by pulsed electron beam surface treatment," *Surface and Coatings Technology*, vol. 206, no. 2-3, pp. 295–304, 2011.

[19] J. X. Zou, K. M. Zhang, T. Grosdidier, and C. Dong, "Analysis of the evaporation and re-condensation processes induced by pulsed beam treatments," *International Journal of Heat and Mass Transfer*, vol. 64, pp. 1172–1182, 2013.

[20] T. Grosdidier, J. X. Zou, N. Stein, C. Boulanger, S. Z. Hao, and C. Dong, "Texture modification, grain refinement and improved hardness/corrosion balance of a FeAl alloy by pulsed electron beam surface treatment in the 'heating mode'," *Scripta Materialia*, vol. 58, no. 12, pp. 1058–1061, 2008.

[21] V. P. Rotshtein, Y. A. Kolubaeva, X. Mei et al., "Effect of conditions of pulsed electron-beam melting for Al (film)/Ti (substrate) systems on phase formation and properties of Ti-Al surface alloys," *Technical Physics Letters*, vol. 38, no. 9, pp. 780–783, 2012.

[22] N. Allain-Bonasso, V. P. Rotshtein, E. Bouzy, L. Germain, Y. F. Ivanov, and T. Grosdidier, "Characterization of Ti-Al surface alloy formed by pulsed electron-beam melting of film-substrate system," *Journal of Physics: Conference Series*, vol. 416, no. 1, Article ID 012007, 2013.

[23] S. R. Dey, E. Bouzy, and A. Hazotte, "EBSD characterisation of massive γ nucleation and growth in a TiAl-based alloy," *Intermetallics*, vol. 14, no. 4, pp. 444–449, 2006.

[24] K. M. Zhang, J. X. Zou, B. Bolle, and T. Grosdidier, "Evolution of residual stress states in surface layers of an AISI D2 steel treated by low energy high current pulsed electron beam," *Vacuum*, vol. 87, pp. 60–68, 2013.

[25] K. M. Zhang, J. X. Zou, T. Grosdidier, C. Dong, and S. Weber, "Ti surface alloying of an AISI 316L stainless steel by low energy high current pulsed electron beam treatment," *Journal of Vacuum Science and Technology A: Vacuum, Surfaces and Films*, vol. 26, no. 6, pp. 1407–1414, 2008.

[26] J. X. Zou, T. Grosdidier, K. M. Zhang, and C. Dong, "Cross-sectional analysis of the graded microstructure in an AISI D2-steel treated with low energy high-current pulsed electron beam," *Applied Surface Science*, vol. 255, no. 9, pp. 4758–4764, 2009.

[27] J. X. Zou, T. Grosdidier, K. M. Zhang, B. Gao, S. Z. Hao, and C. Dong, "Microstructures and phase formations in the surface layer of an AISI D2 steel treated with pulsed electron beam," *Journal of Alloys and Compounds*, vol. 434-435, pp. 707–709, 2007.

[28] G. Shao, T. Grosdidier, and P. Tsakiropoulos, "The metastable disordered γ (TiAl) phase and its ordering process in a rapidly solidified equiatomic TiAl alloy with vanadium addition," *Scripta Metallurgica et Materiala*, vol. 30, no. 7, pp. 809–814, 1994.

[29] L. L. Meisner, M. G. Ostapenko, A. I. Lotkov, and A. A. Neiman, "Surface microstructure and B2 phase structural state induced in NiTi alloy by a high-current pulsed electron beam," *Applied Surface Science*, vol. 324, pp. 44–52, 2015.

[30] J. Kim, S. S. Park, and H. W. Park, "Corrosion inhibition and surface hardening of KP1 and KP4 mold steels using pulsed electron beam treatment," *Corrosion Science*, vol. 89, pp. 179–188, 2014.

[31] J. W. Murray, J. C. Walker, and A. T. Clare, "Nanostructures in austenitic steel after EDM and pulsed electron beam irradiation," *Surface and Coatings Technology*, vol. 259, pp. 465–472, 2014.

[32] J. X. Zou, K. M. Zhang, T. Grosdidier et al., "Orientation-dependent deformation on 316L stainless steel induced by high-current pulsed electron beam irradiation," *Materials Science and Engineering A*, vol. 483-484, no. 1-2, pp. 302–305, 2008.

[33] J. W. Murray and A. T. Clare, "Repair of EDM induced surface cracks by pulsed electron beam irradiation," *Journal of Materials Processing Technology*, vol. 212, no. 12, pp. 2642–2651, 2012.

[34] M. Yamaguchi, D. R. Johnson, H. N. Lee, and H. Inui, "Directional solidification of TiAl-base alloys," *Intermetallics*, vol. 8, no. 5-6, pp. 511–517, 2000.